1983

Lifetime of the 2p state in He II

Gordon W. F. Drake
University of Windsor

J. Patel

A. Van Wijngaarden

Lifetime of the 2p state in He II

G. W. F. Drake*

Lawrence Berkeley Laboratory, University of California, Berkeley, California 94720

J. Patel and A. van Wijngaarden

Department of Physics, University of Windsor, Windsor, Ontario, Canada N9B 3P4

(Received 29 July 1983)

When a beam of spin-polarized metastable $He^+(2s_{1/2})$ ions is quenched by an electric field $\vec{E}$, the emitted radiation intensity contains an asymmetry term proportional to $(\hat{k}\cdot\hat{E})(\vec{P}\cdot\hat{k}\times\hat{E})$, where $\vec{P}$ is the spin-polarization vector and $\hat{k}$ is the direction of observation. The resulting asymmetry is nearly proportional to the level width of the $2p_{1/2}$ state in He^+. The measured asymmetry $0.007\,602\,7\pm0.000\,020\,3$ corresponds to a lifetime $\tau_{2p}=(0.9992\pm0.0026)\times10^{-10}$ sec, in fair agreement with the theoretical value $\tau_{2p}=0.9972\times10^{-10}$ sec.

I. INTRODUCTION

Although the lifetimes of hydrogenic energy levels can be calculated from first principles to high precision, there have been no experimental checks at significantly better than the $\pm1\%$ level of accuracy.[1] The purpose of this paper is to report a measurement of the $2p$ lifetime in He^+ at the $\pm0.26\%$ level of accuracy. The result provides the most precise test of theory to date in an atomic system where the theoretical lifetime is accurately known. The method of measurement is closely related to the anisotropy method of measuring the Lamb shift as discussed previously.[2,3] The present experiment is sensitive to the width of the $2p$ state, rather than the Lamb shift.

The results have a direct bearing on the recent high precision ($\pm0.1\%$) measurements of lifetimes in neutral Li and Na by Gaupp et al.[4] Their values are about 0.8% larger than the best theoretical calculations. Assuming that their experimental values are correct, the agreement with theory obtained in the present experiment suggests that the source of the discrepancy lies in the accuracy of the many-electron wave functions used for Li and Na, rather than basic radiation theory.

The method of measurement used in the present work is novel in that it exploits an interference effect in the electric field quench radiation of a beam of spin-polarized He^+ ions in the metastable $2s_{1/2}$ state. The angular distribution of the Stark-induced Ly-α quenching radiation possesses an anisotropy of about 1.5% which is proportional to the level width Γ of the $2p$ state. The experiment, therefore, consists of measuring an intensity ratio in two perpendicular directions at a single point along the ion beam, rather than measuring an exponential decay curve as a function of position along the beam. Thus the accuracy is not limited by unknown cascade contributions or beam-bending effects, as is sometimes the case in beam-foil measurements of atomic lifetimes.

In the following section, the theory of angular distributions of Ly-α quenching radiation and its relationship to the $2p$-level width is briefly reviewed. This is followed by

Secs. III and IV dealing with the experimental details and the analysis of systematic errors. Finally, Secs. V and VI present the results and discussion.

II. THEORY

A. Basic formalism

The theory of angular distributions in the electric field quenching radiation of hydrogenic ions has been described in detail previously, and is only briefly summarized here.[5,6] If the quench radiation is observed with photon polarization insensitive detectors, then the emitted intensity depends only upon the relative orientations of the three vectors $\vec{k}$, $\vec{P}$, and $\vec{E}$, where $\vec{k}$ is the photon wave vector ($|\vec{k}|=\omega/c$) pointing in the direction of propagation, $\vec{P}$ is the electron spin-polarization vector of the ion beam ($|\vec{P}|\leq1$), and $\vec{E}$ is the electric field vector. $\hat{E}$ and $\hat{k}$ are the corresponding unit vectors. The emitted intensity per unit solid angle in an arbitrary observation direction $\hat{k}$ is then

$$I(\hat{k})=\frac{\alpha k}{4\pi}[J_0(\hat{k})-3\,\mathrm{Im}(V^*_{1/2}V_{3/2})(\hat{k}\cdot\hat{E})(\vec{P}\cdot\hat{k}\times\hat{E})$$

$$+\overline{M}\,\mathrm{Re}(2V_{1/2}+V_{3/2})(\vec{P}\cdot\hat{k}\times\hat{E})$$

$$+2\overline{M}\,\mathrm{Im}(V_{1/2}-V_{3/2})(\hat{k}\cdot\hat{E})]\,, \qquad (2.1)$$

where

$$J_0(\hat{k})=\tfrac{1}{2}\,|\,V_{1/2}+2V_{3/2}\,|^2[1-(\hat{k}\cdot\hat{E})^2]$$

$$+\tfrac{1}{2}\,|\,V_{1/2}-V_{3/2}\,|^2[1+(\hat{k}\cdot\hat{E})^2]+\overline{M}^2\,, \qquad (2.2)$$

$$V_j=\frac{|\vec{E}|}{3}\frac{\langle1s\,|z\,|2p\rangle\langle2p\,|z\,|2s\rangle}{E(2s_{1/2})-E(2p_j)+i\Gamma/2}\,, \quad j=\tfrac{1}{2},\tfrac{3}{2}$$

$$(2.3)$$

in the limit of weak fields where first-order perturbation theory applies and $\overline{M} = \langle 1s \mid M \mid 2s \rangle$ is the matrix element of the relativistic magnetic dipole operator. Equations (2.1) and (2.2) do not include negligibly small contributions from magnetic quadrupole transitions via the $2p_{3/2}$ state or other relativistic corrections of relative order $(\alpha Z)^2$.

The terms in (2.1) are written in order of decreasing magnitude. The first two terms in J_0 are the dominant electric field quenching terms, while the last one gives a very small contribution from spontaneous magnetic dipole transitions to the ground state, which we neglect. The present experiment is designed to measure the second term in (2.1), which we refer to as the $E1$-$E1$ damping term. Since it depends on the imaginary part of $V^*_{1/2}V_{3/2}$, it is proportional to the level width Γ of the $2p$ state. The relatively small contributions from the last two terms of (2.1) average to zero under reversal of the electric field direction, and so do not contribute to the field-averaged signal. The terms of interest which remain after field averaging are therefore

$$I(\hat{k}) = \frac{\alpha k}{4\pi}[J_0(\hat{k}) - 3\operatorname{Im}(V^*_{1/2}V_{3/2})(\hat{k}\cdot\hat{E})(\hat{P}\cdot\hat{k}\times\hat{E})] .$$

$$(2.4)$$

B. Angular distributions

The geometry of the experiment is such that $\vec{P}$ and $\hat{E}$ are orthogonal, and $\hat{k}$ lies in the perpendicular plane through $\hat{E}$ as shown in Fig. 1. Let θ be the angle between $\hat{k}$ and $\hat{E}$ as shown in the figure. If the intensity in the direction $\theta = \pi/2$ is renormalized to unity, then the J_0 term of (2.4) has the angular distribution

$$\mathscr{L}(\theta) = 1 + [2R/(1-R)]\cos^2\theta , \qquad (2.5)$$

where R is the anisotropy

$$R = \frac{\mathscr{L}(0) - \mathscr{L}(\pi/2)}{\mathscr{L}(0) + \mathscr{L}(\pi/2)} \qquad (2.6)$$

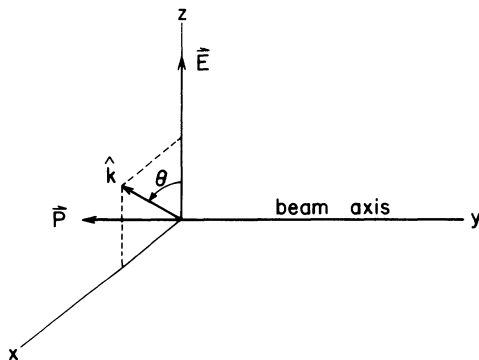used previously to measure the Lamb shift. Using the in-

FIG. 1. Geometry of the experiment showing the electric field vector $\vec{E}$ in the z direction, the spin-polarization vector $\vec{P}$ in the negative y direction, and the direction of observation $\hat{k}$ in the xz plane.

TABLE I. Input data for the calculation of the damping asymmetry.

$E(2s_{1/2}) - E(2p_{1/2})$	14 042.05 MHz
$E(2p_{3/2}) - E(2p_{1/2})$	175 594.0 MHz
$\Gamma(2p)$	1.0028×10^{10} sec^{-1}

put data in Table I, and including small field-dependent corrections,[5] it has the value $R = 0.118\,003$ at our operating field of $E = 246.71$ V/cm. Thus

$$\mathscr{L}(\theta) = 1 + 0.267\,58\cos^2\theta . \qquad (2.7)$$

With the same normalization, the $E1$-$E1$ damping term in (2.4) has the angular distribution

$$\gamma(\theta) = \pm 0.017\,282 \mid \vec{P} \mid \cos\theta\sin\theta . \qquad (2.8)$$

The $(-)$ sign applies if $\vec{P}$ is oriented as shown in Fig. 1, and the $(+)$ sign applies if $\vec{P}$ is reversed. The total-field reversed average intensity is

$$I(\theta) = \mathscr{L}(\theta) + \gamma(\theta) . \qquad (2.9)$$

Polar diagrams for $\mathscr{L}(\theta)$ and $\gamma(\theta)$ are shown in Fig. 2, where the anisotropy in $\mathscr{L}(\theta)$ and the relative magnitude of $\gamma(\theta)$ have been greatly exaggerated. The He$^+$ ion beam passes through the origin into the page, and P is either parallel or antiparallel to the beam velocity as shown. The four channeltrons labeled A,B,C,D view the radiation simultaneously in all four directions. The radiation patterns are invariant under reversal of $\hat{E}$, but $\gamma(\theta)$ reverses sign if $\hat{E}$ is rotated by $\pi/2$ or $\vec{P}$ is reversed. $\mathscr{L}(\theta)$ is invariant under both these operations along the channeltron viewing axes at $\theta = \pi/4$, $3\pi/4$, $5\pi/4$, and $7\pi/4$.

C. The $E1$-$E1$ damping signal

The above analysis shows that the intensity difference between any pair of adjacent counters is sensitive only to the $\gamma(\theta)$ term in (2.9). Using (2.4), the anisotropy, defined by

$$A = \frac{I(\pi/4) - I(3\pi/4)}{I(\pi/4) + I(3\pi/4)} \qquad (2.10)$$

is

$$A = \frac{3\operatorname{Im}(V^*_{1/2}V_{3/2})}{2I_0(\pi/4)} . \qquad (2.11)$$

In the limit of weak fields, this reduces to

$$A = \frac{3\Gamma[E(2p_{3/2}) - E(2p_{1/2})]}{4\Delta^2_{3/2} - 2\Delta_{1/2}\Delta_{3/2} + 7\Delta^2_{1/2} + 11\Gamma^2/4} \qquad (2.12)$$

independent of $\mid \vec{E} \mid$. Here $\Delta_j = E(2s_{1/2}) - E(2p_j)$. For the input data in Table I, the theoretical value of A at zero field strength is $0.007\,620\,9$. The small finite electric field correction at 246.71 V/cm reduces this to $0.007\,618\,2$. Relativistic corrections are of the order 0.01%, and are too small to affect the present results.
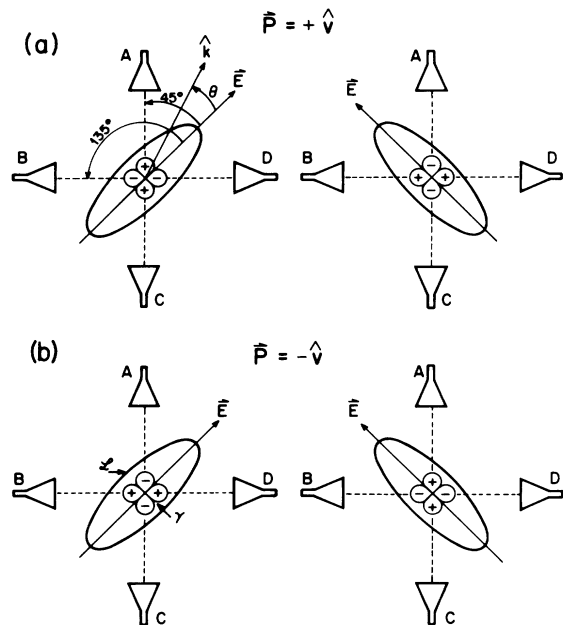
FIG. 2. Polar diagrams for two electric field directions of the two main contributions (not to scale) to the quench radiation for a spin-polarized $He^+(2s)$ beam traveling through the origin, into the page of the paper, for (a) a spin-polarization vector $\vec{P}$ parallel to the beam velocity, and (b) a spin-polarization vector $\vec{P}$ antiparallel to the beam velocity. In arbitrary intensity units the distributions $\mathscr{L}(\theta)=1+0.267\,58\cos^2\theta$ and $\gamma(\theta)=1.7282 \times 10^{-2}\,|\vec{P}|\,\cos\theta\sin\theta$ represent the main quench radiation and the $E1$-$E1$ damping radiation.

Also, an axial magnetic field of 12.9 G was applied to the ion beam during the course of the experiment. The direct effect on A was calculated and found to be a negligible -0.005%. However, it has an indirect effect on the data analysis as discussed in Sec. IV.

The quantity directly measured in the experiment is the intensity ratio

$$r = \frac{I(\pi/4)}{I(3\pi/4)} \ . \tag{2.13}$$

Since it is related to A by $A = (r-1)/(r+1)$, its theoretical value is $r = 1.015\,353$. The relationship between the relative errors in r and A is

$$\frac{\delta r}{r} = \left| \frac{r^2-1}{2r} \right| \frac{\delta A}{A}$$

$$\simeq 0.0152\frac{\delta A}{A} \ . \tag{2.14}$$

Thus a measurement of A (i.e., Γ) to an accuracy of 0.1% requires a measurement of r to 15 parts per million.

III. EXPERIMENTAL

A. Overall plan

The apparatus shown in Fig. 3 is similar to that in our previous[6] experiments but the observation region has been substantially modified with the view of reducing systematic errors. Briefly, a 126-keV $He^+(2s_{1/2})$ ion beam, after passing a prequencher and a collimator, enters into the quenching cell proper and is then monitored with a Faraday cup. The collimator limits the beam diameter to 1.5 mm but still allows radial fluctuations of ± 0.25 mm from the central axis. The quenching cell consists of four metal rods mounted on insulators in a quadrupole arrangement. The static electric quenching field, which always makes an angle of either $\pi/4$ or $3\pi/4$ with any of the observa-
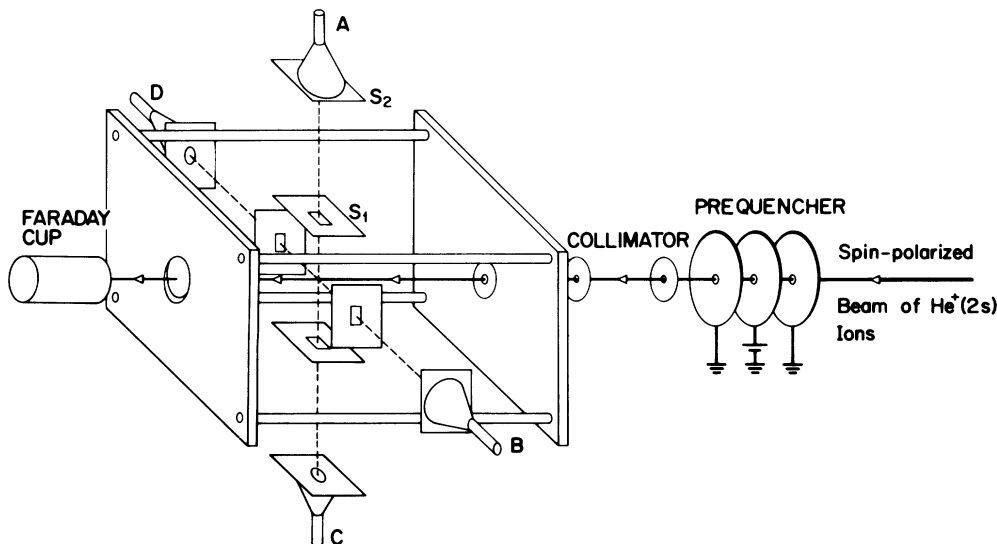

FIG. 3. Schematic diagram of the apparatus. Dimensions are given in the text.

tion axes (see Fig. 2), is obtained by grounding two of the diagonally located opposite quadrupole rods and by applying opposite polarities to the other. Care was taken in the construction of the Faraday cup. Repeller plates suppress the escape of secondary electrons and a beryllium plate for the beam dump at the back of the cup reduces back-scattering of primary ions to a minimum.

The prequencher potentials are only switched on for noise determinations. They are sufficiently strong to destroy virtually all the metastable $He^+(2s_{1/2})$ ions in the beam by quenching.

With the aid of a spin polarizer, the spin-polarization vector can be set at either $\vec{P} = +\hat{v}$ or $\vec{P} = -\hat{v}$ to a high degree of precision. To prevent disorientation of the spin direction, the earth's magnetic field perpendicular to the beam direction is canceled with Helmholtz coils, and to ensure a sharp definition of the y axis a relatively strong magnetic field of 12.9 G (on the average) is applied parallel to the beam direction over the regions of the collimator and quenching cell.

B. Electric field; beam deflection

As the beam traverses the quenching cell it experiences a transverse electric field along the beam or y axis which reaches a maximum (E_0) in the observation region at $y = y_0$. The method[2] for calculating the field has been previously described and Fig. 4 shows the y dependence of the field for our dipole geometry. The field E_0 in the observation region is given by

$$E_0 = (0.6264 \pm 0.0001)\frac{V}{a}$$ (3.1)

in V/cm. Here $a = 2.032$ cm is half the distance between the centers of adjacent rods, each with a diameter of 1.270
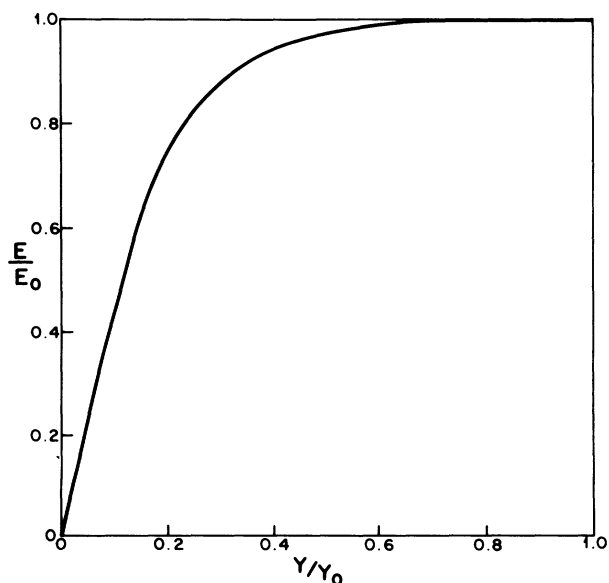

FIG. 4. y dependence of the electric field on the beam axis in the quenching cell. E_0 is the electric field in the observation region centered about y_0.

cm, and V is the magnitude of the potential in volts for the opposite polarities on two diagonally located rods. At our operating potential of 800.3 V, the field has the value $E_0 = 246.7$ V/cm.

In the observation region the beam has obtained a transverse velocity component in the direction of the field given by

$$\frac{v_t}{v_y} = \frac{E_0 y_0}{2Va} \int_0^1 \left| \frac{E}{E_0} \right| d\left| \frac{y}{y_0} \right|.$$ (3.2)

The value of the integral is 0.8493 and at $y_0 = 7.620$ cm one finds that for a beam energy $eV_a = 126$ keV corresponding to a beam velocity $v_y = 2.46 \times 10^8$ cm/sec, $v_t = 1.56 \times 10^6$ cm/sec. At y_0 the beam deflection is 0.21 mm.

C. Photon-detection system

The Ly-α quench radiation (304 Å) is simultaneously observed in four perpendicular directions by photon counters A, B, C, and D (Fig. 3). Counting times are normalized to a preset beam flux, using the output current of the Faraday cup. The photon collimator is shown in Fig. 5. The dimensions of the beam diameter δ, the width α of rectangular slit S_1, the diameter d of aperture S_2, and the other dimensions are

$$\delta = 0.15 \pm 0.03 ,$$

$$\alpha = 0.635 \pm 0.001 ,$$

$$d = 1.016 \pm 0.002 ,$$

$$a = 7.112 \pm 0.002 ,$$

$$b = 21.895 \pm 0.005 ,$$

all measured in cm.

In our earlier work[3] the photon counters consisted of channeltron detectors which were found to become non-linear at high counting rates due to saturation effects. A new photon counter was developed which consists of a
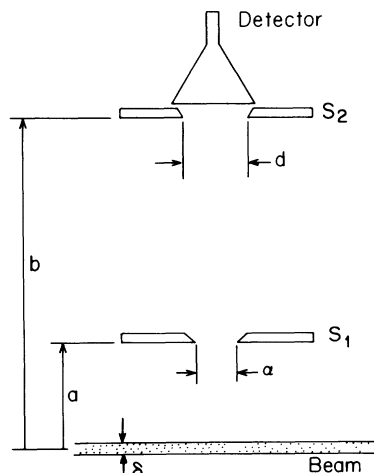

FIG. 5. Schematic diagram of the detector slit system of Fig. 3. The dimensions are given in the text.

compact electron multiplier (Schlumberger, Model 510-00-16-M2) whose conversion dynode has been replaced by a highly uniform custom-built (Galileo Optics) channel-tron cone. The detectors are insensitive to photon polarization and are highly linear. The entrance apertures to the channeltron cones are covered with thin aluminum foils which are transparent to the radiation but stop low-energy particles that are formed by the interaction of the fast ion beam with the remaining gas in the quenching cell. The foils reduce the noise counting rate by about a factor of 50. The remaining noise is proportional to the residual pressure and at the operating pressure of 5×10^{-8} Torr the signal-to-noise ratio is 100:1. Since most of the noise arises from the relatively strong component of ground-state He^+ ions, the signal-to-noise ratio improves rapidly with increasing field strength.

IV. SYSTEMATIC ERRORS AND DATA ANALYSIS

A complete experimental cycle consists of simultaneously recording the total number of counts in a prescribed time period for each of the four counters and for each of the four electric field orientations (see Fig. 2). A study of the systematic effects discussed below defines a unique way of combining the resulting 16 independent measurements (plus 16 more with $\vec{P}$ reversed) so that all but axial magnetic field corrections cancel out to first order. Such complete cancellations can only be achieved with the use of a four-detector system.

A. Systematic asymmetries

1. Angular uncertainties in detector position

The machining tolerance used in the construction of the quenching cell leads to angular uncertainties in the location of the detectors of $\Delta\theta \simeq 0.02°$. The corresponding uncertainty in r is

$$\delta r / r \simeq 0.004\,08\,\Delta\theta$$
$$= 8.2 \times 10^{-5} \tag{4.1}$$

and is invariant under rotation of $\vec{E}$ by 90°. The corresponding uncertainty in A is $\pm 0.5\%$. However, the sign of the error reverses when $\vec{P}$ reverses, and hence the error cancels out to first order in $\Delta\theta$. Second-order effects are negligibly small.

2. Small stray fields

The same analysis applies as above, provided that the stray field does not reverse when $\vec{P}$ reverses. Specific magnetic field corrections that are invariant under reversal of $\vec{P}$ are discussed separately below.

3. Ion-beam drift

Although the ion beam is well collimated along the central axis of the quenching cell, beam drift and machining tolerances introduce angular uncertainties as large as

$\Delta\theta \simeq 0.01°$ which do not cancel out under reversal of $\vec{P}$ or field rotation. However, with four counters, the error does cancel out to first order when signals are averaged over pairs of opposite counters.

4. Variations in measured ion-beam current

The last two terms in Eq. (2.1), which reverse sign under reversal of $\vec{E}$, cancel out of the field-reversed average count rate only if the two signals are properly normalized. One cannot safely use the total beam current measured in the Faraday cup to define equal counting periods because the beam strikes a different spot on the beryllium back plate under field reversal and, after prolonged bombardment, different spots acquire slightly different sensitivities. The correct procedure is to count for equal time periods with sufficiently frequent reversals of field direction that small beam current fluctuations average out.

5. Axial magnetic field effects

The direction of the axial magnetic field $\vec{B}$ in the quenching cell defining the direction of the spin-polarization vector $\vec{P}$ was always set parallel to $\vec{P}$, and so reversed when $\vec{P}$ reversed. The magnitude of $\vec{B}$ was varied from one run to another from 10 to 20 G with a weighted average value of 12.9 G.

Although a magnetic field of this magnitude has a negligible direct effect on the damping anisotropy, it has a number of indirect effects. Firstly, since the ion beam acquires a small transverse velocity v_t [see Eq. (3.2)] in the direction of $\vec{E}$, it experiences an additional $\vec{v} \times \vec{B}$ field of

$$E_m = v_t B / c \tag{4.2}$$

which is perpendicular to $\vec{E}$ such that the total electric field is always rotated counterclockwise by a small angle when $\vec{B}$ is parallel to the beam velocity and clockwise when $\vec{B}$ is reversed. Secondly, the $\vec{B}$ field is not quite homogeneous, but has a small divergence in the beam direction of $\partial B_y / \partial y = -0.50$ G/cm. The resulting electric field in the rest frame of the He^+ ions at a distance R from the y axis equal to the beam deflection in the observation region is

$$E(R) = \frac{1}{2} \frac{v_y}{c} \frac{\partial B}{\partial y} R \ . \tag{4.3}$$

This field always points in the opposite direction to E_m. With $E_m = 0.201$ V/cm and $E(R) = 0.013$ V/cm, the net rotation angle is

$$\Delta\theta = [E_m - E(R)] / |\vec{E}|$$
$$= 0.0437° \ . \tag{4.4}$$

Thirdly, the $\vec{B}$ field slightly perturbs the axial symmetry of the channeltron cones of the photon detectors. Consequently, photoelectrons released from one side of the cone may be more efficiently collected than from the other. This effect is equivalent to a slight angular displacement of the detector.

The corrections introduced by the above three effects are all invariant under reversals of $\vec{E}$ and $\vec{P}$ (since $\vec{B}$ reverses with $\vec{P}$) and so do not cancel out. While the first two can be accurately calculated, the third cannot. Therefore, all three are lumped together and measured directly as a residual instrumental asymmetry, as described in Sec. IV C.

B. Method of data analysis

We now combine the data in such a way that all systematic errors but residual magnetic field effects cancel out to first order. The four counters are labeled A,B,C,D as shown in Fig. 2, and for compactness of notation, $(A/B)_\theta$ denotes the intensity ratio I_A/I_B, and θ specifies the direction of $\vec{E}$ relative to its starting position between counters A and D, as shown in the upper-left corner of Fig. 2. Thus $\theta=0,\pi/2,\pi,3\pi/2$ for the four field orientations.

Starting with counters A and B, first form the product

$$\tilde{r}^2=(A/B)_0(B/A)_{\pi/2} . \tag{4.5}$$

Then $\tilde{r}^2$ is independent of the relative efficiencies of counters A and B, and is a first approximation to the true experimental value of r^2. Second, average over all field orientations to obtain

$$r_{AB}=\frac{1}{2}\left\{\left[\left[\frac{A}{B}\right]_0\left[\frac{B}{A}\right]_{\pi/2}+\left[\frac{A}{B}\right]_0\left[\frac{B}{A}\right]_{3\pi/2}\right.\right.$$
$$\left.+\left[\frac{A}{B}\right]_\pi\left[\frac{B}{A}\right]_{\pi/2}+\left[\frac{A}{B}\right]_\pi\left[\frac{B}{A}\right]_{3\pi/2}\right]^{1/2}$$
$$=\frac{1}{2}\left\{\left[\left[\frac{A}{B}\right]_0+\left[\frac{A}{B}\right]_\pi\right]\left[\left[\frac{B}{A}\right]_{\pi/2}+\left[\frac{B}{A}\right]_{3\pi/2}\right]\right\}^{1/2} . \tag{4.6}$$

Next, construct analogous averages for the other counter pairs and form

$$r_+=\tfrac{1}{4}(r_{AB}+r_{BC}+r_{CD}+r_{DA}) \tag{4.7}$$

for a given orientation of $\vec{P}$. Finally, average over reversal of $\vec{P}$ to find

$$r_0=(r_++r_-)/2 . \tag{4.8}$$

Equation (4.8) must still be corrected for noise by subtracting the noise counts for each detector from the corresponding signals. The noise is defined as the signal still observed after the beam of metastables is destroyed with the prequencher.

C. Residual instrumental asymmetry measurement

The residual systematic asymmetries for the apparatus due to the axial magnetic field can be measured by repeating the experiment with an unpolarized ion beam. Since r should then theoretically be unity, the instrumental correction Δ is determined from

$$r_{\text{inst}}=1+\Delta . \tag{4.9}$$

The quantity Δ should then be subtracted from r_0 to obtain

$$r=r_0-\Delta . \tag{4.10}$$

The statistical error in r (or r_{inst}) from photon counting is

$$\delta r=\frac{r}{2}\left[1+\frac{p}{2}(1+\sqrt{n}\,)\right](N_A^{-1}+N_B^{-1}+N_C^{-1}+N_D^{-1})^{1/2} , \tag{4.11}$$

where the N's are the numbers of signal counts for each detector, p is the fractional noise, and n is the number of successive signal measurements between each noise measurement. It follows that a statistical uncertainty of $\delta r_{\text{inst}}=4\times10^{-5}$ requires 6×10^8 counts per detector for each $\vec{B}$ direction. At our counting rate of 2×10^3 sec^{-1} per detector, this would take a few thousand hours.

However, since Δ scales linearly with $|\vec{B}|$, the counting time was reduced by a factor of 4 by roughly doubling $|\vec{B}|$ from 12.9 to 23.45 G. The results shown in Table II were then rescaled back to the actual magnetic fields used in the different runs to measure r_0. The Δ values for both B directions were each measured several times with an average of 7.35×10^5 photon counts per measurement, for a combined total of 1.72×10^9 counts. The standard deviation $\delta\Delta_{\text{expt}}$ in the result is in agreement with Eq. (4.11) for a noise level of 0.65%. This level is a factor of 2 lower than that for a spin-polarized beam because one of the $m_s=\pm\frac{1}{2}$ components is missing in the latter case. The agreement between the standard deviations shows that errors are no worse than can be expected from counting statistics alone. The magnetic-field-induced rotation of $\vec{E}$ discussed in Sec. IV A 5 predicts the value $\Delta=65\times10^{-5}$. The difference of about 18×10^{-5} between this value and the ones from Table II is due to the magnetic field effect on the detectors and can be accounted for if the field rotates the center gravity for photon detection by 0.02°. This rotation is small compared to the acceptance angle $\Delta\theta=2.5°$ of the channeltron cones.

The actual measurements on the damping ratio were obtained in several runs on different days with different magnetic field settings. Thus the scaled Δ corrections that were subtracted from r_0 differed from one run to another. The scaled average values corresponding to a 12.9 G average field for $\hat{B}=+\hat{v}$ and $\hat{B}=-\hat{v}$ are

$$\Delta_+=(27.06\pm3.87)\times10^{-5} ,$$

$$\Delta_-=(25.22\pm3.76)\times10^{-5} ,$$

respectively.

TABLE II. Results for the instrumental asymmetry $r_{\text{inst}}=1+\Delta$ at $B=23.45$ G.

	Number of measurements	Δ (average)	$(\delta\Delta)_{\text{expt}}$	$(\delta\Delta)_{\text{theor}}$
$\hat{B}=\hat{v}$	1149	48.2×10^{-5}	$\pm6.9\times10^{-5}$	$\pm7.0\times10^{-5}$
$\hat{B}=-\hat{v}$	1192	46.0×10^{-5}	$\pm6.9\times10^{-5}$	$\pm6.9\times10^{-5}$

D. Dead-time correction

The electronic dead time τ for the photon counting system results in a loss of counts. The corresponding fractional decrease in the asymmetry is given by[2]

$$\frac{\delta A}{A} = \frac{1}{2}\tau\left\langle\frac{n}{T}\right\rangle(1-A^2) \tag{4.12}$$

where $\langle n/T \rangle$ is the total counting rate for a pair of counters, averaged over a complete measurement. Using Eq. (2.14) and the theoretical value $r = 1.01535$, the decrease in the damping ratio becomes

$$\delta r = 7.74 \times 10^{-3}\tau\left\langle\frac{n}{T}\right\rangle . \tag{4.13}$$

The dead time for each of the four photon counters was set at the same value. For the majority of the runs $\tau = (40\pm1)$ nsec. The dead-time correction was applied to each measurement separately. The weighted-average correction is

$$\delta r = (0.17\pm0.02)\times10^{-5}$$

for the average counting rate $\langle n/T \rangle = 5365$ sec^{-1} in adjacent pairs of detectors.

E. Pressure correction

Exchange of electrons between the spin-polarized ions in the beam and the residual gas along the 120-cm-long flight path from the spin polarizer to the observation region destroys the spin-polarization vector and lowers the observed damping ratio. To measure the correction, the pressure was raised with hydrogen gas by a factor 15 from the normal operating pressure of 5×10^{-8} Torr to 7.5×10^{-7} Torr and, as expected, the noise level increased by the same factor. Damping ratios were then measured in two separate runs, one for each of the spin-polarization vectors, with each run containing 200 separate measurements and 1.5×10^8 photon counts. The two results were then used to extrapolate the precision measurements at 5×10^{-8} Torr to zero pressure. The resulting corrections,

$$\Delta r_+ = (1.3\pm1.0)\times10^{-5} ,$$

$$\Delta r_- = (1.8\pm1.3)\times10^{-5} ,$$

are consistent with each other. The average-pressure correction becomes

$$\Delta r = (1.55\pm0.82)\times10^{-5} . \tag{4.14}$$

F. Solid-angle correction

The correction factor for the solid angle by which the observed asymmetry must be multiplied is similar to that for our earlier[2] work on the Lamb shift and is given by

$$A = A_{\mathrm{obs}}\left[1+(1-R)\frac{\alpha^2+\frac{3}{4}d^2}{12(b-a)^2}+\frac{\frac{3}{4}d^2}{6b^2}+\frac{\delta^2}{8b^2}\right] . \tag{4.15}$$

Here $R = 0.118$ is the $0°-90°$ Lamb-shift asymmetry and

the other parameters refer to the photon slit system of Fig. 5. Their substitution into the previous equation yields the correction factor 1.000 671 for A. Using Eq. (2.14) this factor corresponds to a correction

$$\Delta r = 1.038\times10^{-5} \tag{4.16}$$

for an r value $r_{\mathrm{theor}} = 1.01535$.

V. EXPERIMENTAL DATA AND STATISTICAL ANALYSIS

In all 3120 individual measurements of r_0 were made for $\vec{P} = +\hat{v}$ and 3281 for $\vec{P} = -\hat{v}$ in 30 different runs on different days. Each measurement contains on the average 7.78×10^5 photon counts for a combined total of 4.98×10^9 counts. The mean and standard deviation from counting statistics of all the measurements for each spin-polarization vector weighted by the number of counts in each measurement are

$$\bar{r} = \sum_{i=1}^{N}\frac{r_i n_i}{n_T} \tag{5.1}$$

and

$$\sigma = \left[\sum_{i=1}^{N}\frac{(r_i-\bar{r})^2 n_i}{n_T(N-1)}\right]^{1/2} , \tag{5.2}$$

where n_i is the number of counts in the ith measurement, n_T is the total number of counts, and N is the number of measurements. The experimental values for $\vec{P} = +\hat{v}$ and $\vec{P} = -\hat{v}$ are (including the Δ correction)

$$r_+ = 1.0153745\pm(0.0000436\pm0.0000003) ,$$

$$r_- = 1.0152174\pm(0.0000427\pm0.0000005) .$$

The experimental standard deviations are the ones from counting statistics alone, and do not include the errors in the Δ corrections. The errors on the standard deviations themselves were found using the "bootstrap" method of Diaconis and Efron.[7] The corresponding theoretical errors from Eq. (4.11) for a noise level $p = 1.2\%$, which was determined after $n = 3$ successive signal measurements, are

$$\sigma_+ = 0.0000432\pm0.0000003 ,$$

$$\sigma_- = 0.0000421\pm0.0000003 ,$$

in satisfactory agreement with the experimental values. It is indeed satisfying that despite the large variations in the magnetic field correction Δ, the fluctuations in data are no worse than what can be expected from counting statistics alone.

Figures 6(a) and 6(b) compare the histograms of the experimental data distributions with the theoretically expected histograms for Gaussian distributions. The χ^2 test of the fits with the mean and the standard deviations as the only adjustable parameters yields $\chi^2_+ = 38.4$ for 52 degrees of freedom and $\chi^2_- = 41.9$ for 51 degrees of freedom, corresponding to confidence levels of 92% and 81%, respectively. The results of runs tests[2] are given in Table III.
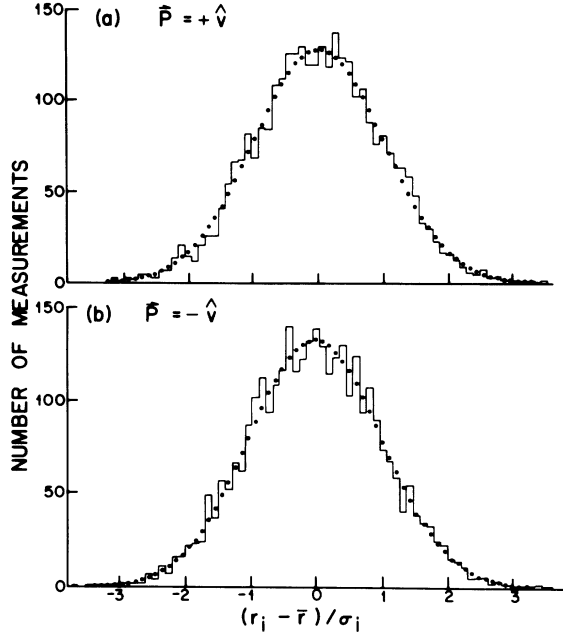
FIG. 6. Histograms for the distribution of the experimental data about the mean in units of the observed standard deviation for each point, for (a) the spin-polarization vector parallel to the beam velocity, and (b) the spin-polarization vector opposite to the beam velocity. The solid circles show the expected bar heights for a Gaussian distribution with the same mean and unit half-width.

The theoretical distribution is based on the assumption that the probability for a measurement to fall above the mean and the probability to fall below the mean are the same ($\frac{1}{2}$). None of these tests reveals statistically significant anomalies in the data.

To account for the large difference,

$$r_+ - r_- = 0.000\,157$$

of nearly four standard deviations, we tabulate in Table IV the ratio measurements for adjacent pairs of photon counters [see Eq. (4.6)]. The statistical error for each ratio is nearly the same with an uncertainty of ± 6 in the last significant figure. One finds that the r values lower substantially when $\vec{P}$ is switched from $+\hat{v}$ to $-\hat{v}$. An anomaly of this type is expected if, on average, the photon-detection system is rotated with respect to the quadrupole assembly from its proper position through an angle $\Delta\theta = 0.019°$, which falls within the construction tolerances of $\Delta\theta = 0.02°$.

TABLE III. Comparison of the observed numbers of low and high runs with the expected number of runs for (a) $\vec{P} = +\hat{v}$ and (b) $\vec{P} = -\hat{v}$.

Run length	Low runs	High runs	Expected number
(a)			
1	379	371	390±17
2	208	210	195±13
3	86	103	98± 9
4	45	41	49± 6
5	27	25	24± 5
6	15	7	12± 3
7	3	4	6.1± 2.4
8	3	4	3.0± 1.7
9	4	4	1.5± 1.2
10	1	2	0.8± 0.9
11	0	0	0.38± 0.61
12	1	1	0.19± 0.44
13	0	0	0.10± 0.31
Total	772	772	780±14
(b)			
1	408	391	410±18
2	212	231	205±13
3	105	111	103± 9
4	47	45	51± 7
5	24	24	26± 5
6	17	12	13± 3
7	3	3	6.4± 2.4
8	4	2	3.2± 1.7
9	0	0	1.6± 1.2
10	2	2	0.8± 0.9
11	0	1	0.40± 0.63
12	1	0	0.20± 0.45
13	0	1	0.10± 0.32
Total	823	823	820±14

Upon inclusion of the errors in the systematic corrections Δ and the other systematic effects summarized in Table V, the damping ratios become

$$r_+ = 1.015\,400\,4 \pm 0.000\,059\,0 ,$$

$$r_- = 1.015\,243\,3 \pm 0.000\,057\,5 .$$

Averaging these eliminates field-rotation errors to first order and yields

$$r = 1.015\,321\,9 \pm 0.000\,041\,2 .$$

The corresponding value of A is $0.007\,602\,7 \pm 0.000\,020\,3$, in agreement with the theoretical value $0.007\,618\,2$.

TABLE IV. Ratio measurements for adjacent pairs of photon detectors.

	r_{AB}	r_{BC}	r_{CD}	r_{AD}
$\vec{P} = +\hat{v}$	1.015 46 (± 6)	1.015 52 (± 6)	1.015 28 (± 6)	1.015 23 (± 6)
$\vec{P} = -\hat{v}$	1.015 21 (± 6)	1.015 41 (± 6)	1.015 23 (± 6)	1.015 02 (± 6)

G. W. F. DRAKE, J. PATEL, AND A. van WIJNGAARDEN

TABLE V. Summary of experimental data and of systematic corrections.

	$\vec{P}=\hat{v}$	$\vec{P}=-\hat{v}$
$r-\Delta$	1.015 372 8 ($\pm5.84\times10^{-5}$)	1.015 215 7 ($\pm5.69\times10^{-5}$)
Finite pressure	0.000 015 5 ($\pm0.82\times10^{-5}$)	0.000 015 5 ($\pm0.82\times10^{-5}$)
Solid angle	0.000 010 4 ($\pm0.01\times10^{-5}$)	0.000 010 4 ($\pm0.01\times10^{-5}$)
Dead time	0.000 001 7 ($\pm0.02\times10^{-5}$)	0.000 001 7 ($\pm0.02\times10^{-5}$)
Total	1.015 400 4 ($\pm5.90\times10^{-5}$)	1.015 243 3 ($\pm5.75\times10^{-5}$)
Average	1.015 321 9 ($\pm4.12\times10^{-5}$)	
A	0.007 602 7 ($\pm2.03\times10^{-5}$)	

VI. DISCUSSION

Using Eq. (2.12) and assuming that the energy differences in Table I are correct, the experimental value of A corresponds to a lifetime $\tau=1/(2\pi\Gamma)$ for the $2p$ state of $\tau_{\text{expt}}=(0.9992\pm0.0026)\times10^{-10}$ sec. This falls within one standard deviation of the theoretical value 0.9972×10^{-10} sec. It is a considerable improvement over the beam-foil result of $(0.98\pm0.05)\times10^{-10}$ sec by Lundin et al.[8] and over our own previous measurement of $(0.988\pm0.013)\times10^{-10}$ sec.[6]

The high-precision lifetime measurements of Gaupp et al.[4] for neutral Li and Na generally lie about 0.8% above theory. Although our result also lies above theory by $(0.20\pm0.26)\%$, a discrepancy as large as 0.8% can al-most certainly be ruled out. Our result confirms basic radiation theory at the $\pm0.2\%$ level, and the source of the discrepancies for Li and Na must be sought elsewhere.

*Permanent address: Department of Physics, University of Windsor, Windsor, Ontario N9B 3P4, Canada.

[1] B. J. Miller, J. R. Fuhr, and G. A. Martin, in *Bibliography on Atomic Transition Probabilities, November 1977 Through March 1980*, Natl. Bur. Stand. Spec. Publ. No. 505 (U.S. GPO, Washington, D.C., 1980).

[2] A. van Wijngaarden and G. W. F. Drake, Phys. Rev. A 17, 1366 (1978).

[3] G. W. F. Drake, S. P. Goldman, and A. van Wijngaarden, Phys. Rev. A 20, 1299 (1982).

[4] A. Gaupp, P. Kuske, and H. J. Andrä, Phys. Rev. A 26, 3351 (1982).

[5] A. van Wijngaarden and G. W. F. Drake, Phys. Rev. A 25, 400 (1982).

[6] A. van Wijngaarden, R. Helbing, J. Patel, and G. W. F. Drake, Phys. Rev. A 25, 862 (1982).

[7] P. Diaconis and B. Efron, Scientific American 248, 116 (1983) and references therein.

[8] L. Lundin, H. Oona, W. S. Bickel, and I. Martinson, Phys. Scr. 2, 213 (1970).